RSC Advances

PAPER

View Article Online
View Journal | View Issue

Cite this: *RSC Adv.*, 2020, **10**, 387

Crystallization behavior and optical properties of isotactic polypropylene filled with α-nucleating agents of multilayered distribution

Shanshan Luo,[a] Liangqiang Wei,[a] Jing Sun,[a] Anrong Huang,[a] Shuhao Qin,[a] Heng Luo,[a] Chengtao Gao,[a] Yu Zheng *[b] and Jiabin Shen[b]

Received 14th November 2019
Accepted 18th December 2019

DOI: 10.1039/c9ra09485g

rsc.li/rsc-advances

Isotactic polypropylene (iPP)-based multilayered composites containing alternating layers of pure iPP and α-nucleating agents (α-NAs)-filled iPP (αPP) were fabricated through layer-multiplying co-extrusion technology. With the manipulation of layer number, a tunable multilayered distribution of α-NAs was achieved and its effect on the crystallization behavior and optical properties of iPP was investigated. When the thickness of an individual iPP layer, which is equal to the distance between adjacent αPP layers, was large, the crystallization process of iPP was governed by homogeneous nucleation, although the crystallization of areas near the layer interfaces was induced by α-NAs. As a result, most iPP formed big spherulites thus a poor clarity. By decreasing the layer thickness *via* multiplying the layer number, the nucleation of iPP was gradually transformed from a homogeneous mode to a heterogeneous mode because of the more and more strong influence of αPP layers on the crystallization process of adjacent iPP layers. Consequently, iPP exhibited similar crystallization behavior compared with αPP. The polarized optical microscopy results further demonstrated that the size of spherulites in iPP was significantly reduced with the increase of layer number, which contributed to the enhancement of transmittance and decline of haze. Accordingly, this work developed a novel approach to tailor the crystallization behavior and optical properties of iPP.

1 Introduction

Materials capable of crystallizing are extremely attractive because their properties can be optimized *via* manipulation of the crystallization progress.[1–5] As one of the most widely applied semicrystalline polymers, isotactic polypropylene (iPP) possesses several extraordinary properties involving good mechanical properties, excellent chemical and moisture resistance, versatile processability and low cost. However, the inherent large spherulites in common iPP always lead to an opacity, which has been regarded as the major obstacle for realizing applications with the requirement of high transparency.[6–9] Hence, a great deal of effort has been made to modify its transparency.

It appears from the existing literature that several approaches could be adopted to optimize the optical property of iPP *via* controlling its crystallization behavior, mainly including increasing the fraction of amorphous phase by chemical synthesis, destroying spherulite texture by hot or cold stretching, and reducing the size of spherulites by inclusion of α-nucleating agents (α-NAs).[10–13] Among them, incorporation of α-NAs is the most effective methodology for endowing iPP with transparency. Some papers have reported that a large reduction of haze occurs in iPP filled with only 0.1–1.0 wt% α-NAs.[14,15] Besides, the optical properties of iPP/α-NAs composites are also significantly influenced by the distribution of α-NAs.[16,17] For instance, Tenma *et al.* produced injection-molded polypropylene with sorbitol-based clarifier which can be self-assembly into fibril by adjusting the applied flow field and thermal history. It was found that the fibril-like α-NAs could induce more tiny spherulites formed, giving a distinct enhancement of transparency.[18,19] In another work, Kobayashi *et al.* achieved fibrous distribution of α-NAs by using 1,3:2,4-bis-*O*-(*p*-methylbenzylidene)-D-sorbitol with self-assembling ability, and successfully developed highly transparent iPP.[20] Accordingly, the confined distribution of α-NAs in iPP such as forming needle or fibril can always optimize the nucleating efficiency thus the clarity.

As another special approach for achieving confined filler distribution, the multilayered structure has attracted tremendous academic attention in the last decades. Particularly, the emergence of layer-multiplying co-extrusion technology, which

[a]*Guizhou Material Industrial Technology Institute, Guizhou Material Technology Innovation Base, National and Local Joint Engineering Research Center for Functional Polymer Membrane Materials and Membrane Processes, Guiyang 550014, China*

[b]*State Key Laboratory of Polymer Materials Engineering, Polymer Research Institute of Sichuan University, Sichuan Provincial Engineering Laboratory of Plastic/Rubber Complex Processing Technology, Chengdu 610065, China. E-mail: zy1990@scu.edu.cn*

can enable the construction of multilayered structure to be more efficient and controllable, brings mass enthusiasm for developing superior properties *via* multilayered distribution of fillers.[21] Many reports have stated that multilayered distribution of fillers exhibited more efficient for modification compared with the random state, that has been applied to prepare composites with outstanding mechanical, electrical, dielectric, barrier, and optical performances.[22–29] However, few studies focusing on the relationship between multilayered distribution of α-NAs and optical properties of iPP are concerned, as far as we know.

In this study, the multilayered distribution of α-NAs was realized by fabrication of multilayered composites containing alternating iPP and α-NAs-filled iPP (αPP) layers through layer-multiplying co-extrusion technology. As illustrated in Fig. 1, the distribution of α-NAs was tailored by changing the number of layers and its effect on the crystallization behaviors and optical properties of iPP was researched schematically. This work firstly related the optical properties of iPP to the multilayer distribution of α-NAs and provided a potential route to fabricate iPP products with tunable transparency.

2 Experimental

2.1 Materials

The iPP homopolymer (F401) with a melt index of 3.0 g/10 min (230 °C, 2.16 kg) and a density of 0.91 g cm^{-3}, was purchased from Yangzi Petrochemical Company Ltd (China). The number- and weight-average molecular weight measured by gel permeation chromatography (GPC, PL-220) at 150 °C were 5.0×10^5 and 1.4×10^5, respectively. The polydispersity was 2.9. The α-nucleating agent (trade name: T5688) was one of sorbitol derivatives and supplied by Xin Hua Plastic Co., Ltd, Dong Guan, China.

2.2 Specimen preparation

The iPP and α-NAs were dried in an oven at 80 °C for 8 h before melt processing. Prior to the layer-multiplying coextrusion, αPP pellets containing 0.7 wt% α-NAs were prepared using a twin-screw extruder. Subsequently, the iPP/αPP multilayered composites were prepared using the layer-multiplying coextrusion system, the fabrication progress of which has been described previously.[30] In this work, the 2-, 4-, 8-, 16-, and 32-layer iPP/αPP multilayered materials were fabricated with 0, 1, 2, 3, 4 layer multiplying elements (LMEs). The temperature profile of the extruder from hopper to die was set as follow: 160, 200, 205, 200 °C, and the temperature of the coextrusion block and LMEs was set at 200 °C. The thickness ratio of iPP and αPP layers was set at 3 : 2 by controlling the feed speed of the two extruders, and the total thickness of each composite was maintained at 1.0 mm. By calculation, the content of α-NAs in the whole iPP/PN multilayered composites was ~0.3 wt%.

2.3 Differential scanning calorimetry (DSC)

The non-isothermal and isothermal crystallization behaviors of the iPP/αPP multilayered composites were examined by differential scanning calorimetry (DSC, Q20, TA Instrument Co., USA) under a nitrogen atmosphere. For non-isothermal crystallization, samples of 6–8 mg were heated to 200 °C and maintained for 5 min to eliminate thermal history. Subsequently, the

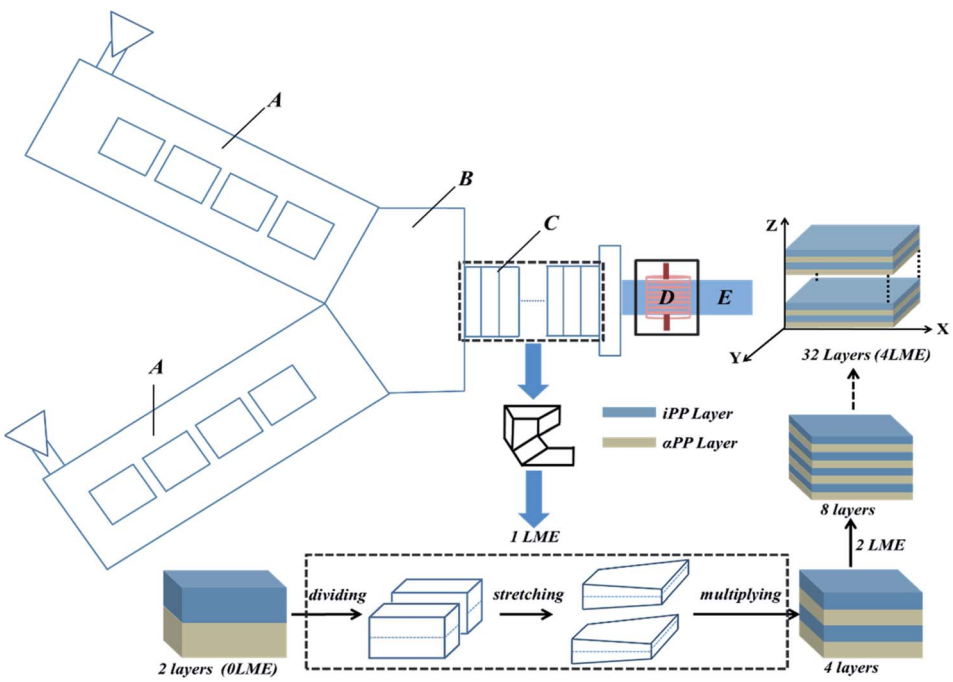

Fig. 1 Schematic of layer-multiplying coextrusion system: (A) single screw extruder; (B) coextrusion block; (C) layer-multiplying elements (LMEs); (D) rolling and cooling block; (E) multilayered extrudate.

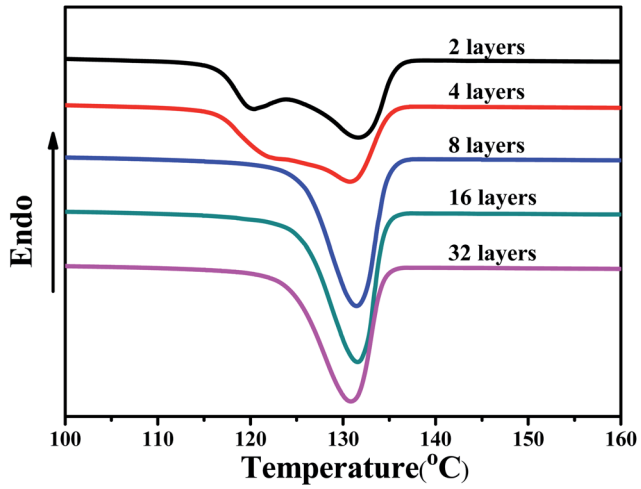

Fig. 2 DSC cooling curves of the iPP/αPP multilayered composites.

samples were cooled down to 80 °C at a cooling rate of 10 °C min^{-1}. The cooling curves were recorded. The first melting procedure of the isothermal crystallization tests was the same with the non-isothermal crystalline process. After erasing the heat history, the samples were cooled down to 133 °C at a cooling rate of 50 °C min^{-1} and maintained this temperature to crystalline completely.

2.4 Polarized optical microscopy (POM)

The polarized optical microscopy (POM) observation was performed on an Olympus BX51 polarizing microscope equipped with an attached camera and a heating cell. A thin slice about 15 μm in thickness was obtained by a microtome from each extrudate along the extrusion direction. For recording the spherulite growth process, each specimen was first heated to 200 °C at a rate of 10 °C min^{-1}, and held at 200 °C for 5 min to eliminate heat history. Then, the samples were rapidly cooled down to 133 °C and maintained at this temperature to crystalline completely. The spherulitic morphology in specimen during crystallization was recorded by a camera.

2.5 Optical properties characterization

The transmittance and haze of each iPP/αPP multilayered materials were investigated by a transmittance/haze measuring machine (Shanghai Precision Instrument Co., China). At least of three specimens for each sample were tested and the average value was calculated.

3 Results and discussion

3.1 Crystallization behaviors

The non-isothermal crystallization behaviors of the iPP/αPP multilayered materials was first investigated by conducting DSC experiments, and the cooling curves were recorded in Fig. 2. The crystallization of multilayered extrudates exhibited strong dependence on layer number (N). When N was 2, there were two distinct crystallization peaks with crystallization temperature (T_c) respectively locating at about 120 and 132 °C: the higher one belonged to αPP because of the heterogeneous nucleation effect induced by α-NAs; the lower one belonged to iPP in which homogeneous nucleation dominated the crystallization process, meaning that the α-NAs have little influence on the crystallization behavior of the thick iPP layers. By increasing the layer number just from 2 to 4, the two crystallization peaks moved close to each other and the low temperature crystallization peak tended to disappear. This revealed that the formation of richer interfaces can reinforce the crystallization inducing effect of nucleating agents dispersed in αPP layers on their adjacent iPP layers. Moreover, the specimen with a larger N than 8 exhibited only one crystallization peak and a T_c close to that of αPP, further indicating that a transformation from homogeneous to heterogeneous nucleation might occur in the crystallization progress of iPP with increasing N.

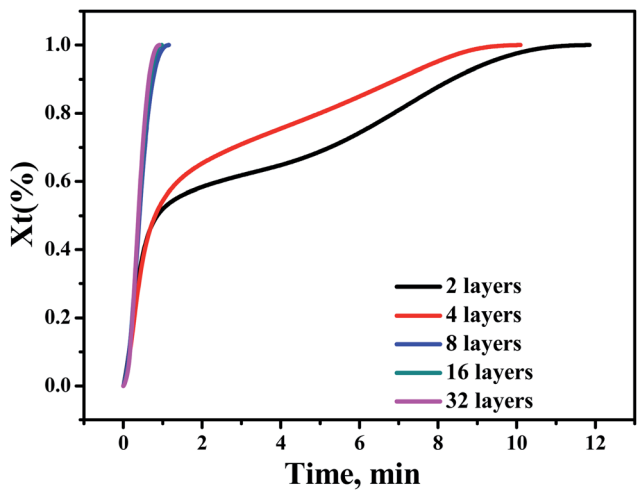

Fig. 3 Relative crystallinity as a function of time for the iPP/αPP multilayered composites.

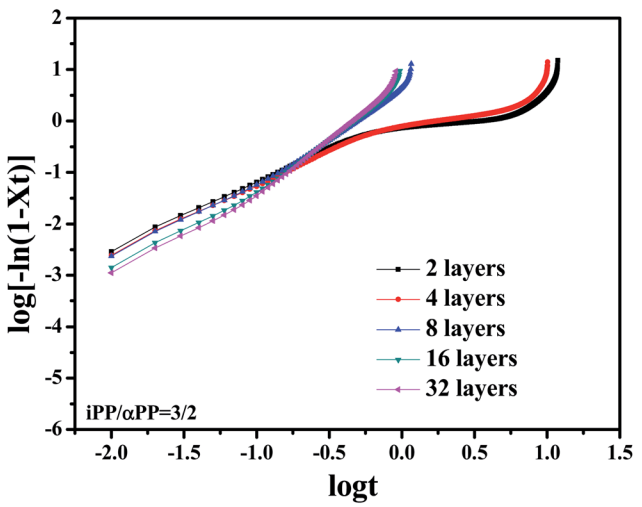

Fig. 4 Avrami plots of the iPP/αPP multilayered composites.

Table 1 Avrami exponent n for iPP/αPP multilayered composites

Layer number	2	4	8	16	32
n	1.4, 4.0	1.4, 3.5	1.9	2.1	1.9

In order to further provide an insight into the relationship between multilayered distribution of α-NAs and crystallization behaviors of iPP, the isothermal crystallization of specimens was also investigated using DSC. Fig. 3 depicts the evolution of relative crystallinity (X_t) with time for the iPP/αPP multilayered composites isothermally crystallized at 133 °C after elimination of thermal history. It can be clearly seen that the curves shifted to the left with the enhancement of N, demonstrating that specimens with larger N cost less time to finish crystallization. It is well established that the crystallization rate with heterogeneous nucleation is faster than that with homogeneous nucleation.[31] Thus, the accelerated crystallization of the sample possessing larger N is well associated with the view proposed above that the crystallization progress of iPP would be gradually governed by heterogeneous nucleation instead of homogeneous nucleation with increasing N.

Besides, the crystallization kinetics of specimens related to N were analyzed by the known Avrami model. The double logarithmic form of Avrami equation is expressed as:[32]

$$\log[-\ln(1 - X_t)] = n \log t + \log k$$

where X_t is the relative crystallinity at time (t), n and k represent the Avrami exponent and crystallization rate constant, respectively. Generally, n as the slope of linear fitting from the plot of $\log[-\ln(1 - X_t)]$ *versus* $\log t$ refers to the nucleation mode of crystallization, and the n value of homogeneous nucleation is usually larger than that of heterogeneous nucleation as the spherulites grow under the same dimensional space.[33] Fig. 4 displays the Avrami plots of iPP/αPP multilayered composites isothermally crystallized at 133 °C, and the corresponding n values were calculated and recorded in Table 1. The iPP/αPP multilayered composites with small N exhibited Avrami curves with two linear regions, thus had two n values referring to the distinct nucleation types. The one larger than 3 should be associated with the homogeneous nucleation of iPP layers, and the lower one should represent the heterogeneous nucleation of αPP layers.[34] This phenomenon was attributed to that the α-NAs in αPP layers had little influence on the crystallization of iPP layers with a large thickness, so that the iPP and αPP layers crystallized with homogeneous and heterogeneous nucleation respectively. By enlarging N, the plots became linear and had a single n value, further reinforcing the conclusion that narrow distance between αPP layers induced the disappearance of homogeneous nucleation in iPP layers and encouraged the whole extrudates to exhibit a similar crystallization behavior to that of αPP.

As discussed above, the multilayered distribution of α-NAs can result in distinct crystallization behavior of iPP by manipulation of layer number. Thus, it is reasonable to deduce that the spherulitic morphology in the iPP/αPP multilayered composites should change with the evolution of N. Fig. 5 displays the POM images of the iPP/αPP multilayered specimens. For the specimen with small N, numerous tiny spherulites nucleated from the α-NAs were homogeneously dispersed in the αPP layers, while a sandwich structure of tiny spherulites/large spherulites/tiny spherulites was clearly observed in the iPP layers such as in the 2-layer sample. This suggested that α-NAs only influenced the area of the iPP located at the layer interfaces, however, the central region of the iPP layers was still controlled by homogeneous nucleation. With the increase of N, the homogeneous nucleation region of iPP got narrower and finally disappeared, replaced by the tiny spherulites. As a result, the specimen with a large N presented a crystal morphology like that observed in the conventional αPP.

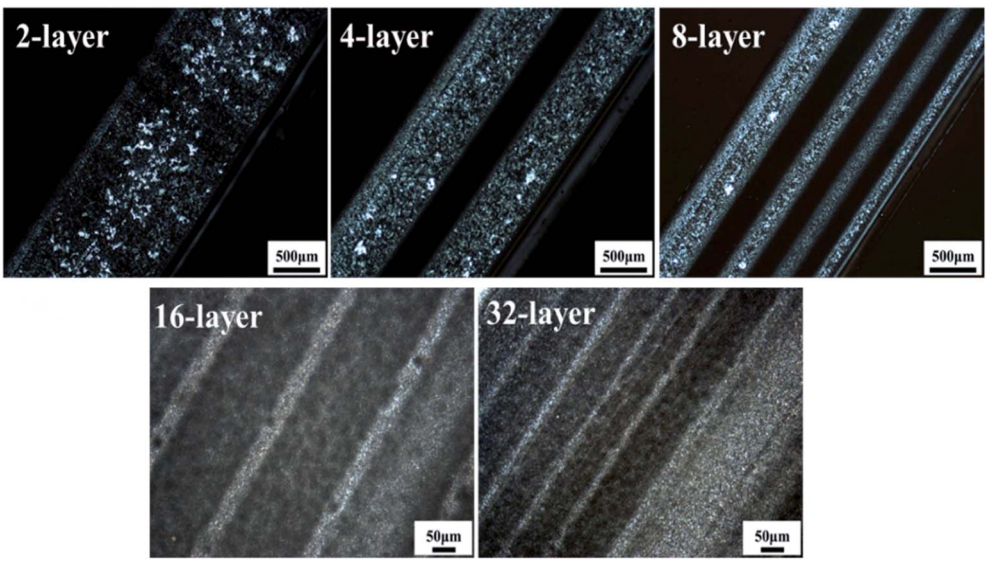

Fig. 5 POM pictures of the multilayered iPP/αPP samples with different layer numbers.

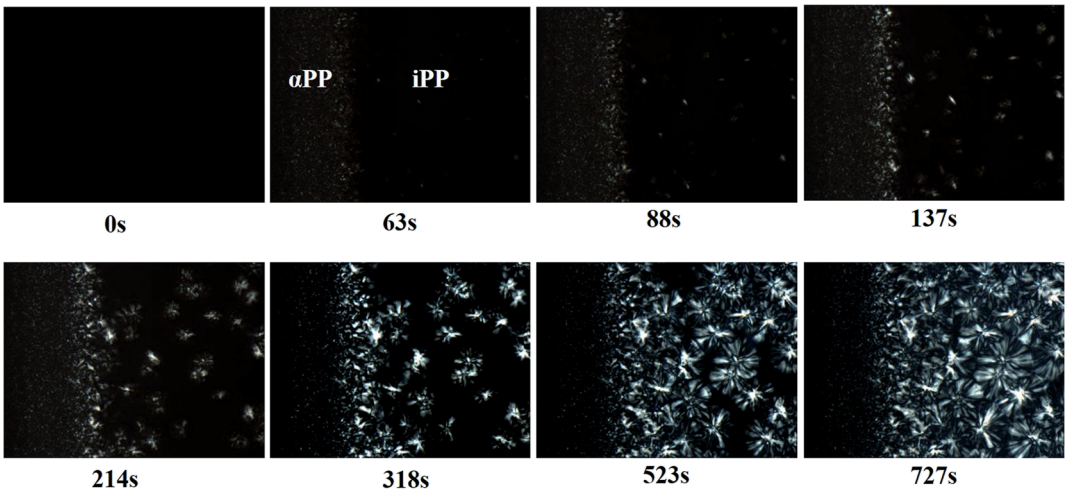

Fig. 6 POM images of the 4-layer iPP/αPP multilayered material isothermally crystallized at 133 °C. Scale bar: 50 μm.

POM equipped with a heating cell was further applied to get a clear observation of the effect of N on the crystal growth of the iPP/αPP multilayered materials. As concluded above, the materials with large N could instantaneously complete crystallization accompanied with the formation of numerous tiny spherulites when the temperature drops down to T_c of 133 °C. Therefore, Fig. 6 only presents the isothermally crystallized process at 133 °C of the 4-layer specimen with large layer thickness. Upon cooling, the αPP layers first crystallized because of the heterogeneous nucleation effect induced by α-NAs and were crammed immediately by tiny spherulites. Meanwhile, the region of iPP around the interfaces which was influenced by the α-NAs also crystallized accompanied with the formation of tiny spherulites, forming an ambiguous interface between iPP and αPP layer. As time progressed, large spherulites gradually appeared in the central region of the iPP layers and the growth of each spherulite was terminated by the other. This further demonstrates that the α-NAs in αPP layers has little influence on the crystallization of iPP layers (especially the central region) in the specimen with a small N.

3.2 Optical properties

Considering that the spherulite size of iPP was reduced with the increase of N, the optical properties of the whole iPP/αPP multilayered composites should be simultaneously tuned. Fig. 7 displays the influence of N on the transmittance and haze of the iPP/αPP multilayered composites. When the N value was larger than 8, the transmittance greatly increased and the haze dramatically declined, which meant enhanced transparency.

The light transmitting mechanisms of the iPP/αPP multilayered composites with different N were also schematically illustrated in Fig. 8. When the iPP layers were thick, the crystallization of iPP layers was barely affected by α-NAs, finally creating large and perfect spherulites. Most incident lights would be scattered by the big spherulites, leading to the deteriorated transmittance and enhanced haze. On the contrast, the diminishing distance between the adjacent αPP layers would strengthen the heterogeneous nucleating effect of α-NAs on the iPP layers, inducing the formation of tiny spherulites. The light can directly pass through the whole extrudates because of the tiny spherulites in both iPP and αPP layers, thus, a transparent iPP based material was successfully developed.

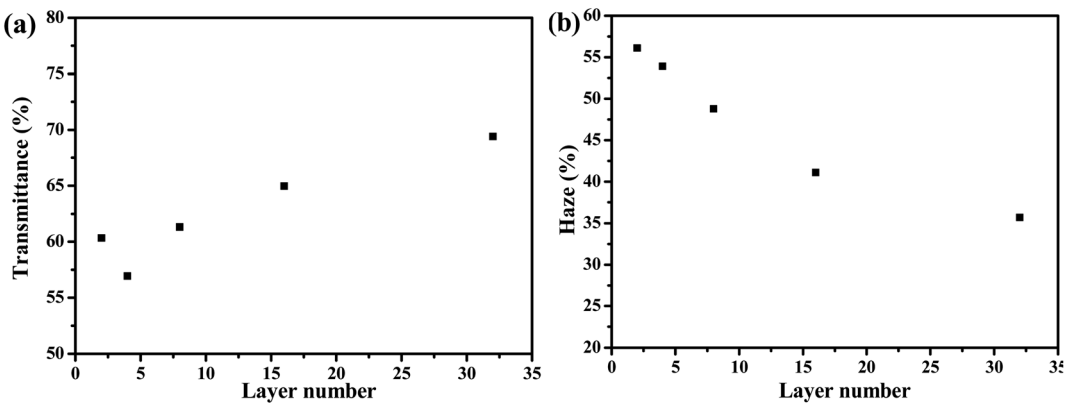

Fig. 7 (a) Transmittance and (b) haze for the iPP/αPP multilayered composites.

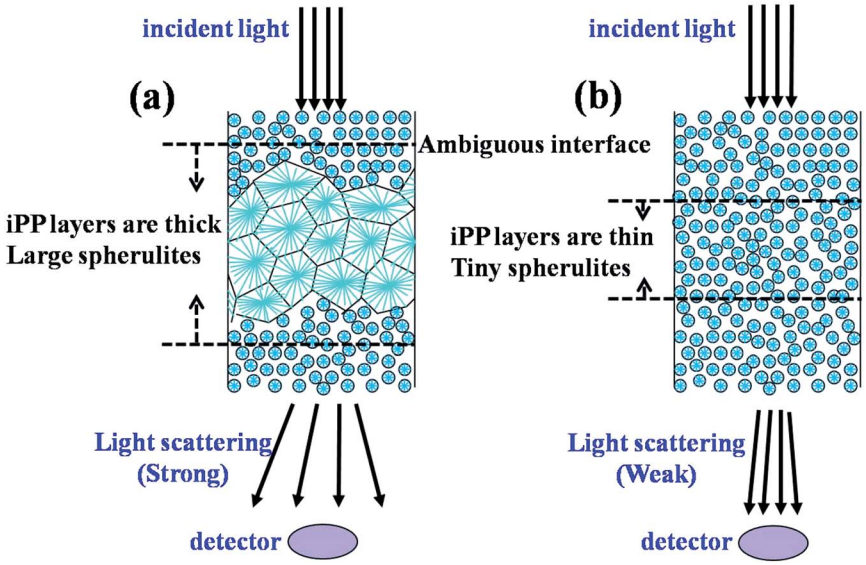

Fig. 8 Schematic of light passing through the iPP/αPP multilayered materials.

4 Conclusions

The well-confined multilayered distribution of α-NAs in iPP was achieved by layer-multiplying co-extrusion technology. The crystallization behaviors and optical properties of the iPP/αPP multilayered composites showed significant dependence on the layer number. At a low layer number, the thick iPP layers crystallized with homogeneous nucleation because of the little effect induced by α-NAs, leading to the formation of big spherulites and a poor clarity. By decreasing the layer thickness with multiplication of layer number, the crystallization of iPP gradually changed from homogeneous nucleation to heterogeneous nucleation, and there were finally only tiny spherulites formed in the whole specimen. With respect to that the light scattering could be weaken by tiny spherulites, the iPP/αPP multilayered composites with thin iPP layers possessed an enhanced transparency. This work firstly related the optical performance to the multilayered distribution of α-NAs and provided a promising route to fabricate iPP with tunable light transmittance performances.

Conflicts of interest

There are no conflicts of interest to declare.

Acknowledgements

The authors gratefully acknowledge the financial support of this work by the Guiyang Baiyun District Science and Technology Plan Project (grant no. [2018] 4), the National Engineering Research Center for Compounding and Modification of Polymer Materials Program (Compounding ke he 201801), National Natural Science Foundation of China (grant no. 21664004), the Guizhou Province Science and Technology Project (grant no. [2018] 3006, [2019] 2849, [2019] 2028, [2019] 5639, [2019] 5636, [2017]4760).

References

1 J. M. Li, Y. W. Du, D. Feng, M. X. Quan and Z. Q. Hu, *Adv. Eng. Mater.*, 1999, **1**, 137.
2 J. M. Li, M. X. Quan and Z. Q. Hu, *Appl. Phys. Lett.*, 1996, **69**, 2356.
3 J. M. Li, *Appl. Phys. Lett.*, 2007, **90**, 041913.
4 L. Chen, X. Li, L. Wang, W. Wang and Z. Xu, *Polym. Compos.*, 2017, **38**, 5–12.
5 W. Li, Z. Xu, L. Chen, M. Shan, X. Tian, C. Yang, H. Lv and X. Qian, *Chem. Eng. J.*, 2014, **237**, 291–299.
6 J. Wang and Q. Dou, *Colloid Polym. Sci.*, 2008, **286**, 699–705.
7 K. Resch, G. M. Wallner, C. Teichert, G. Maier and M. Gahleitner, *Polym. Eng. Sci.*, 2006, **46**, 520–531.
8 S. Luo, L. Yi, Y. Zheng, J. Shen and S. Guo, *Eur. Polym. J.*, 2017, **89**, 138–149.
9 S. Luo, P. Yi, Y. Xiong, J. Shen and S. Guo, *J. Appl. Polym. Sci.*, 2016, **133**, 42844.
10 A. Funaki, K. Kondo and T. Kanai, *Polym. Eng. Sci.*, 2011, **51**, 1068–1077.
11 J. Wang and Q. Dou, *Polym. Int.*, 2008, **57**, 233–239.
12 Z. Horváth, A. Menyhárd, P. Doshev, M. Gahleitner, G. R. Vörös, J. Varga and B. Pukánszky, *ACS Appl. Mater. Interfaces*, 2014, **6**, 7456–7463.
13 K. Resch, G. M. Wallner, C. Teichert and M. Gahleitner, *Polym. Eng. Sci.*, 2007, **47**, 1021–1032.
14 K. Bernland, T. Tervoort and P. Smith, *Polymer*, 2009, **50**, 2460–2464.
15 P. M. Kristiansen, A. Gress, P. Smith, D. Hanft and H. W. Schmidt, *Polymer*, 2006, **47**, 249–253.
16 M. Blomenhofer, S. Ganzleben, D. Hanft, H. W. Schmidt, M. Kristiansen, P. Smith, K. Stoll, D. Mäder and K. Hoffmann, *Macromolecules*, 2005, **38**, 3688–3695.

17 A. Menyhárd, M. Gahleitner, J. Varga, K. Bernreitner, P. Jääskeläinen, H. Øysæd and B. Pukánszky, *Eur. Polym. J.*, 2009, **45**, 3138–3148.
18 M. Tenma, N. Mieda, S. Takamatsu and M. Yamaguchi, *J. Polym. Sci., Part B: Polym. Phys.*, 2008, **46**, 41–47.
19 M. Tenma and M. Yamaguchi, *Polym. Eng. Sci.*, 2007, **47**, 1441–1446.
20 T. Kobayashi and T. Hashimoto, *Bull. Chem. Soc. Jpn.*, 2005, **78**, 218–235.
21 X. Zhang, Y. Xu, H. Wu, J. Shen, R. Chen, Y. Xiong, J. Li and S. Guo, *Prog. Polym. Sci.*, 2019, **89**, 76–107.
22 S. Luo, Y. Zheng, Z. Zheng, H. Wu, J. Shen and S. Guo, *Chem. Eng. J.*, 2019, **355**, 710–720.
23 Y. Yu, S. Yang, H. Yu, J. Li and S. Guo, *Macromolecules*, 2017, **50**, 5098–5106.
24 W. Gao, J. Shen and S. Guo, *Polym. Eng. Sci.*, 2014, **54**, 1471–1476.
25 Y. Gao, X. Gao, J. Li and S. Guo, *Compos. Sci. Technol.*, 2018, **158**, 175–185.
26 X. Ji, D. Chen, J. Shen and S. Guo, *Chem. Eng. J.*, 2019, **362**, 190–198.
27 M. Gupta, Y. Lin, T. Deans, E. Baer, A. Hiltner and D. A. Schiraldi, *Macromolecules*, 2010, **43**, 4230–4239.
28 J. Zhu, J. Shen, S. Guo and H. J. Sue, *Carbon*, 2015, **84**, 355–364.
29 L. Xia, H. Wu, S. Guo, X. Sun and W. Liang, *Composites, Part A*, 2016, **81**, 225–233.
30 C. Li, T. Jiang, J. Wang, S. Peng, H. Wu, J. Shen, S. Guo, X. Zhang and E. Harkin-Jones, *ACS Sustainable Chem. Eng.*, 2018, **6**, 6247–6255.
31 J. E. K. Schawe, F. Budde and I. Alig, *Polymer*, 2018, **153**, 587–596.
32 V. Khoshkava, H. Ghasemi and M. R. Kamal, *Thermochim. Acta*, 2015, **608**, 30–39.
33 S. Zhao, Z. Cai and Z. Xin, *Polymer*, 2008, **49**, 2745–2754.
34 M. Mucha, J. Marszałek and A. Fidrych, *Polymer*, 2000, **41**, 4137–4142.